ORIGINAL ARTICLE

Numerical assessment of interstand tensions in continuous hot rolling processes of flat and long products

Christian Overhagen[1]

Abstract

The paper deals with the calculation of interstand tensions in continuous rolling mills.In the rolling mill industry, continuous measurement and data collection of roll forces, roll torques, temperatures and roll velocities is possible. However, the important process parameter of interstand tensions is not directly measurable and no direct calculation of the interstand tensions is possible. The interstand tensions couple the effects of subsequent roll gaps and should therefore by known for a holistic recalculation of the process. It is straightforward to calculate the effects of the tensions on roll forces, torques and the stock velocity. The inverse problem of calculating the acting interstand tensions including their effects from the process parameters is of greater interest but also of a higher complexity, because the interactions between all the stands in the rolling mill must be regarded. The present paper aims at filling this research gap by presenting a mathematical model to solve the inverse problem by a linearization of the tensions influences in the rolling mill. The present model does not require measured roll forces or torques to find the interstand tensions, only the rotational velocities of the rolls and the rolling parameters (material, temperature, pass schedule or pass design) must be known. Tension-dependent spread is considered by an empirical sub-model. Results are shown for the tension distributions in strip and rod mills. The results indicate that the present friction conditions and the entry size of the rolled stock have a high impact on the tension distributions.

1 Introduction

Hot rolled steel products are essential for our modern society. When we look at the typical process routes for the production of high-quality parts for the automotive, aerospace and other industries, we shall recognize that more than 95 % of the crude steel produced is deformed in one or more hot rolling mills during its production cycle. There is no other process to provide the necessary high production capacities, where at the same time the microstructure of the processed material is refined in a cyclic manner.

Nowadays, the hot rolling processes for flat and long products have reached a state in which an economic production is only possible by the use of multistand continuous rolling operations. In these, we are faced with the challenge that the material is deformed in multiple roll gaps at the same time. These continuous rolling processes are bound to the law of continuity, i.e. a constant volume flux in all stands of the rolling mill.

Therefore, a careful adjustment of the rotational speeds of the respective roll sets is necessary. The elementary rolling theory, first introduced by von Karman [7] provides a mathematical basis for designing the necessary roll speeds. By the identification of a neutral point in the roll gap, it became possible to relate the velocities of the roll surface and the rolled stock to one another and explaining the existence of a forward slip between the stock exit and the circumferential roll velocities.

The first to understand that the neutral point offers a method of coupling the stress and velocity distributions was Orowan [19]. Therefore, interstand tensions acting at the roll gap entry and exit influence the neutral point position and therefore the revolutional speeds of the rolls if the volume flux remains a constant.

Even if the rotational speed adjustments are done with high precision, process variations can lead to variations in the

✉ Christian Overhagen
  christian.overhagen@uni-due.de

1   Chair of Metallurgy and Metal Forming, Research and
    Teaching Field Metal Forming, University of Duisburg-Essen,
    Forsthausweg 2, 47057 Duisburg, Germany

neutral point positions, therefore causing interstand tensions to arise which affect the rolling process. Too low a tension can lead to compressive stresses in the rolled stock, causing a massive mill failure by producing a cobble of the rolled stock. Too high a tension may lead to a rupture of the rolled stock in the most fatal case. Therefore, it is the current aim of the rolling mill personell to keep the interstand tensions moderately low all the time. However, a targeted use of interstand tensions can provide a means of controlling the rolled cross sections and therefore be beneficial for the rolling process. As the interstand tensions cannot be measured directly, a mathematical model must be found from which the actual interstand tensions can be calculated. The core purpose of the current paper is the presentation of such a model, which allows the interstand tension stresses to be calculated from the rolling parameters. This is accomplished by means of the static-kinematic coupling in the roll gap provided by the elementary rolling theory. The application of the model is shown by a wide range of industrial rolling examples on hot strip, flat bars and wire rod.

For the rolling processes of narrow flat bars and long products, it will be seen from the examples presented in this paper, that the lateral spread is of much greater interest than for rolling of wide flat products. Therefore, the direct influences of the interstand tensions on the lateral spread are taken into account for these processes. Mauk already provided a mathematical model for this tension influence on the actual deformations [14], which serves as a submodel in the current research.

Spuzic presented a framework for digitization of rolling groove geometries using polynomial approximations [24], aiming at a general digitization of industrial rolling mill records. To enable a full digital evaluation of such industrial data records, the calculation of the interstand tensions which acted during the recorded rolling operations is a crucial factor to enable the process to be fully recalculated by a physically based process model.

A calculation of the effects of the interstand tensions on the stress distribution for plane strain rolling processes can be easily carried out using slab method approaches of rolling [1, 7], but the inverse calculation of the interstand tensions that act in a specific rolling process is much more complicated. The problem gains extra complexity, when three-dimensional rolling process with lateral spread is considered, which is especially the case for rolling of long products.

The presented calculation method is based on a stepwise linearization of the tension influences on the rotational roll speeds, based on the basic equations of the rolling theory. Assembled for all stands of the rolling mill, a linear system of equations follows which is solved in order to calculate an approximation to the actual acting tensions. This methodology was chosen to attain a mathematical solution which is consistent with the analytical rolling theory which has proven to deliver a realistic assessment of the tension influences. In this way, the necessary information to ensure close product tolerances and high operational safety to the physical process can be supplied.

2 Method for the inverse calculation of interstand tensions

In the present analysis, von Karman's theory of rolling is employed in the form given by Alexander [1] and later employed by Chen et al. [2]. For the flat rolling case treated by Alexander, a rectangular sheet or strip section is reduced from the initial height h_0 to the final height h_1 by passing through a gap formed between two cylindrical rollers as shown in Fig. 1.

The width of the rolled product is w_0 at the roll gap entry and w_1 at the roll gap exit. Hence it follows that the cross sections of the rolled stock are $A_0 = h_0 w_0$ at the entry and $A_1 = h_1 w_1$ at the exit. The length of the deformation zone (in rolling direction) is given as:

$$l_d = \sqrt{R\Delta h - \frac{\Delta h^2}{4}} \tag{1}$$

with $\Delta h = h_0 - h_1$. The arc of contact is formed by the roll radius R between the entry and exit planes EE' and AA'. The contact angle or bite angle α_0 is given as:

$$\cos\alpha_0 = 1 - \frac{\Delta h}{2R} \tag{2}$$

Each cross-sectional plane in the roll gap volume can be addressed by a specific angle α with $0 \le \alpha \le \alpha_0$. $\alpha = \alpha_0$ corresponds to the entry plane, where $\alpha = 0$ corresponds to the exit plane. We may also define a related angle:

$$\alpha' = \frac{\alpha}{\alpha_0} \tag{3}$$

The rolled stock enters the roll gap at the initial velocity v_0 and exits the roll gap at the final velocity v_1. The rolls rotate at the angular velocity ω, resulting in the circumferential velocity $v_c = \omega R$. v_0 and v_1 are connected to the cross sections by the law of a constant volume flux:

$$\dot{V} = Av = A_0 v_0 = A_1 v_1 \tag{4}$$

There is a specific angle α_N called the neutral angle, where the horizontal velocity of the stock material is equal to the horizontal component of the circumferential roll velocity, $v(\alpha_N) = v_c \cos\alpha_N$. In the roll gap, at the neutral angle the cross-section $A_N = A(\alpha_N)$ is present.
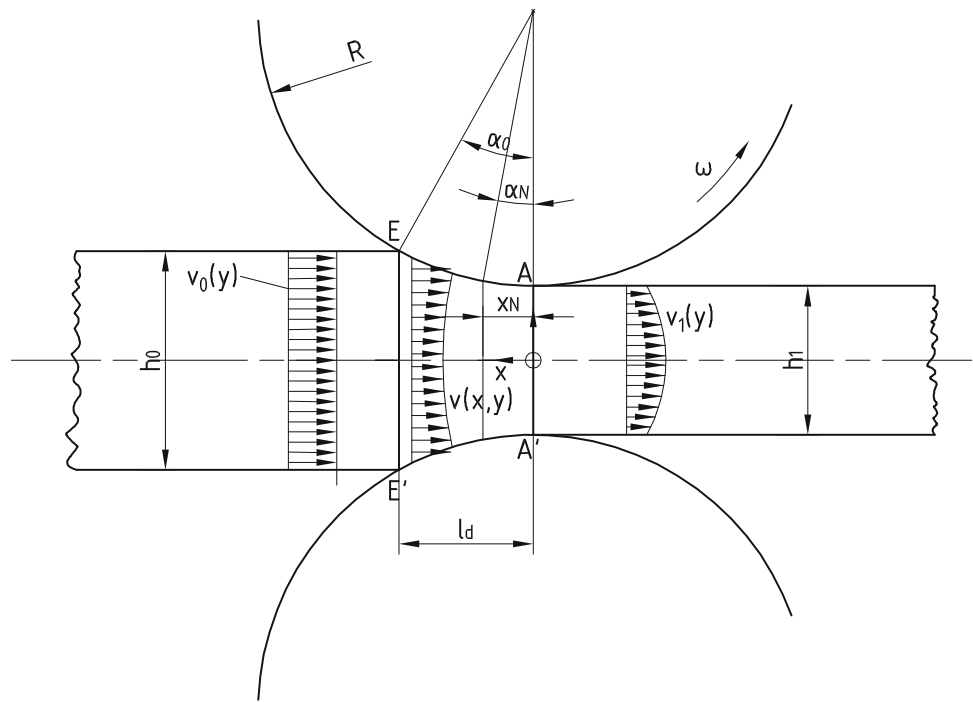
We may rewrite Eq. 4 for the neutral angle:

$$\dot{V} = Av = A_1 v_1 = A(\alpha_N) v(\alpha_N) = A_N v_c \cos \alpha_N \tag{5}$$

From Eq. 5, it may be deduced that the roll gap exit velocity differs from the circumferential roll velocity. We define a forward slip κ:

$$\kappa = \frac{v_1 - v_c}{v_c} = \frac{A_N}{A_1} \cos \alpha_N - 1 \tag{6}$$

The forward slip is typically in the order of magnitude of 3 to 9 % for hot rolling. It is basically the forward slip and the neutral angle which lets us find a connection between the acting interstand tensions and rotational velocity of the rolls, as will be shown in the next chapters.

2.1 The rolling model for a single rolling stand

Von Karman's approach of a force equilibrium at the strip element in the roll gap yields an ordinary differential equation, which is expressed in the most general form with the horizontal stress σ_x, the strip height h, the normal stress between rolls and rolled material σ_N, the frictional shear stress τ_F and the roll surface inclination α [7]:

$$\frac{d(\sigma_x h)}{dx} = 2 \left(\sigma_N \tan \alpha \pm \tau_F \right) \tag{7}$$

In the present analysis, we will utilize Alexander's rolling theory exemplarily because it is a systematic numerical

scheme for the integration of Eq. 7, noting the model could be implemented with any other rolling theory which permits the calculation of the local normal stress in the roll gap. Alexander introduced the vertical force decomposition along with Tresca's yield criterion and two possible friction laws. He provided numerically-solvable ordinary differential equations for the cases of slipping friction and sticking friction. For slipping friction, the frictional shear stress depends upon the normal stress σ_N and is given as:

$$\tau_F = \mu \sigma_N \tag{8}$$

Alexander's differential equation for σ_N in the case of slipping friction is now given in the following way:

$$\frac{d\sigma_N}{d\alpha} = f_1(\alpha) \sigma_N(\alpha) + f_2(\alpha) \tag{9}$$

Where the functions f_1 and f_2 are given as:

$$f_1(\alpha) = \pm \frac{\mu}{\cos \alpha} \frac{\left(\frac{2R'}{h} + \frac{1}{\cos \alpha} \right)}{1 \mp \tan \alpha} \tag{10}$$

$$f_2(\alpha) = \frac{\frac{2R'}{h} k_f \sin \alpha + \frac{dk_f}{d\alpha}}{1 \mp \tan \alpha} \tag{11}$$

For sticking friction, τ_F is not expressed in relation to σ_N, but in terms of the flow stress in pure shear k. It is related to

the flow stress in uniaxial tension k_f in the following way:

$$\tau_F = k = \frac{k_f}{\sqrt{3}} \tag{12}$$

Also, $\frac{d\sigma_N}{d\alpha}$ does not depend on σ_N. Alexander provided the differential equation for sticking friction according to:

$$\frac{d\sigma_N}{d\alpha} = g_1(\alpha)k_f(\alpha) + g_2(\alpha) \tag{13}$$

In Eq. 13, the functions $g_1(\alpha)$ and $g_2(\alpha)$ are given as:

$$g_1(\alpha) = \frac{2R'\kappa(\alpha)}{h}\sin\alpha \pm g_3(\alpha) \tag{14}$$

$$g_2(\alpha) = \kappa(\alpha)\frac{dk_f}{d\alpha} \tag{15}$$

$$\kappa(\alpha) = 1 \pm \frac{1}{2}\tan\alpha \tag{16}$$

$$g_3(\alpha) = \left(\frac{R'}{h}\cos\alpha + \frac{1}{2\cos^2\alpha}\right) \tag{17}$$

The work roll flattening is accounted for by Hitchcock's model [6]. It assumes an increased radius of the arc of contact R' given by:

$$\frac{R'}{R} = 1 + \frac{C_H F}{w_m(h_0 - h_1)} \tag{18}$$

With the roll force F and the elastic constant C_H of the roll material:

$$C_H = \frac{16}{\pi}\frac{1 - \nu^2}{E} \tag{19}$$

To enable the numerical solution of these ordinary differential equations, the yield stress k_f must be known at any point of the arc of contact. In addition, we require the information of the first derivative of the flow stress evaluation $\frac{dk_f}{d\alpha}$. In the present analysis, we utilize an analytical flow curve equation which describes k_f as a function of the the parameters true strain φ, strain rate $\dot{\varphi}$ and temperature ϑ:

$$k_f = k_f(\varphi, \dot{\varphi}, \vartheta) \tag{20}$$

The needed derivative $\frac{dk_f}{d\alpha}$ is calculated from the partial derivatives of the flow curve equation according to:

$$\frac{dk_f}{d\alpha} = \frac{\partial k_f}{\partial\varphi}\frac{d\varphi}{d\alpha} + \frac{\partial k_f}{\partial\dot{\varphi}}\frac{d\dot{\varphi}}{d\alpha} + \frac{\partial k_f}{\partial\vartheta}\frac{d\vartheta}{d\alpha} \tag{21}$$

We may now calculate the distribution of the strain rate in the roll gap according to:

$$\dot{\varphi} = \frac{d\varphi}{dt} = \frac{d\varphi}{d\alpha}\frac{d\alpha}{dt} = -\frac{2v(\alpha)\tan\alpha}{h(\alpha)} \tag{22}$$

For the derivative of the flow stress in the roll gap $\frac{dk_f}{d\alpha}$, the expression $\frac{d\dot{\varphi}}{d\alpha}$ is needed. We can differentiate Eq. 22 with respect to α and get:

$$\frac{d\dot{\varphi}}{d\alpha} = -\frac{2}{h}\frac{dh}{d\alpha}v(\alpha)\tan\alpha + \frac{2}{h}\frac{dv}{d\alpha}\tan\alpha + \frac{2}{h}v(\alpha)\frac{1}{\cos^2\alpha} \tag{23}$$

The particular flow stress function which we use for hot rolling is due to Mauk and Gottschling [16] as their function No. 8 and given as:

$$k_f(\varphi, \dot{\varphi}, \vartheta) = k_0 \cdot e^{m_1\vartheta} \cdot \dot{\varphi}^{m_2 + m_5\vartheta} \cdot \varphi^{m_3} \cdot e^{m_4\varphi} \tag{24}$$

We can write out the partial derivatives of Eq. 24 analytically:

$$\frac{\partial k_f}{\partial\varphi} = k_0\varphi^{m_3-1}\dot{\varphi}^{m_2+m_5\vartheta}e^{m_4\varphi+m_1\vartheta}(m_3 + m_4\varphi) \tag{25}$$

$$\frac{\partial k_f}{\partial\dot{\varphi}} = k_0\varphi^{m_3}\dot{\varphi}^{m_2+m_5\vartheta-1}e^{m_4\varphi+m_1\vartheta}(m_2 + m_5\vartheta) \tag{26}$$

$$\frac{\partial k_f}{\partial\vartheta} = k_0\varphi^{m_3}\dot{\varphi}^{m_2+m_5\vartheta}e^{m_4\varphi+m_1\vartheta}(m_1 + m_5\ln\dot{\varphi}) \tag{27}$$

Now, the needed derivative of the flow stress is given in terms of:

$$\frac{dk_f}{d\alpha} = \frac{\partial k_f}{\partial\varphi}\frac{d\varphi}{d\alpha} + \frac{\partial k_f}{\partial\dot{\varphi}}\frac{d\dot{\varphi}}{d\alpha} + \frac{\partial k_f}{\partial\vartheta}\frac{d\vartheta}{d\alpha} \tag{28}$$

As the contact time between rolls and rolled stock will be very low, we can usually disregard the last term in Eq. 28 and operate with a mean rolling temperature. This temperature may be calculated from the following equations, regarding the heat transport between rolls and rolled stock, the heat generation due to forming heat and the heat losses due to radiation between the passes. The radiation loss can be calculated as follows:

$$\Delta\vartheta_R = \frac{\varepsilon C_R t_R C}{A\rho(\vartheta)c_p(\vartheta)}\left[\left(\frac{T_S}{100}\right)^4 - \left(\frac{T_a}{100}\right)^4\right] \tag{29}$$

In Eq. 29, ε is the radiation coefficient, C_R is the Stefan-Boltzmann constant, t_R is the radiation time in seconds, C is the circumference of the rolled cross section, A is the area of the rolled cross section, $\rho(\vartheta)$ is the temperature-dependent mass density and $c_p(\vartheta)$ is the temperature-dependent specific heat capacity of the rolled material. The absolute initial temperature of the rolled stock in K is T_S and the absolute ambient temperature is T_a. Equation 29 is applied between the passes of a continuous rolling mill arrangement. In the roll gaps, the two effects of heat conduction and forming heat take place at the same time. The temperature loss due to conduction is modelled in terms of:

$$\Delta\vartheta_C = \frac{2l_d w_m k_L(\vartheta_S - \vartheta_{RC})}{c_p(\vartheta)\rho(\vartheta)\dot{V}} \tag{30}$$

In Eq. 30, l_d is the contact length as defined in Fig. 1, w_m is the mean width of the rolled stock in the roll gap, ϑ_S is the stock temperature and ϑ_{RC} is the temperature of the roll core.

This calculation method of thermal transmission is due to Pawelski for hot rolling and forging processes [21]. The model takes into account the heat transport through an oxide scale layer with the thickness s_c. The heat transfer coefficient k_L describes the heat transport between the roll core and the core of the rolled stock. It is given as

$$k_L = \frac{\sqrt{c_p(\vartheta)\lambda(\vartheta)\rho(\vartheta)}}{2\sqrt{t_c}} \left\{ \frac{e^{n^2}}{n} \left[1 - \Phi(n) \right] - \frac{1}{n} + \frac{2}{\sqrt{\pi}} \right\}$$

(31)

The dimensionless figure n is given as:

$$n = \frac{2\lambda_c}{\sqrt{c_{pR}\lambda_R\rho_R}} \frac{\sqrt{t_c}}{s_c}$$

(32)

In these equations, c_p, λ and ρ are the temperature-dependent specific heat, thermal diffusivity and mass density of the stock material, respectively. c_{pR}, λ_R and ρ_R are the respective material properties of the roll material and λ_c is the thermal diffusivity of the oxide scale layer. The thermophysical properties of the oxide scale are taken from [8].

Fig. 2 Kinematic-static coupling in the roll gap; a) Stress Distributions with neutral point; b) Velocity distributions with neutral point; c) Strain rate distribution
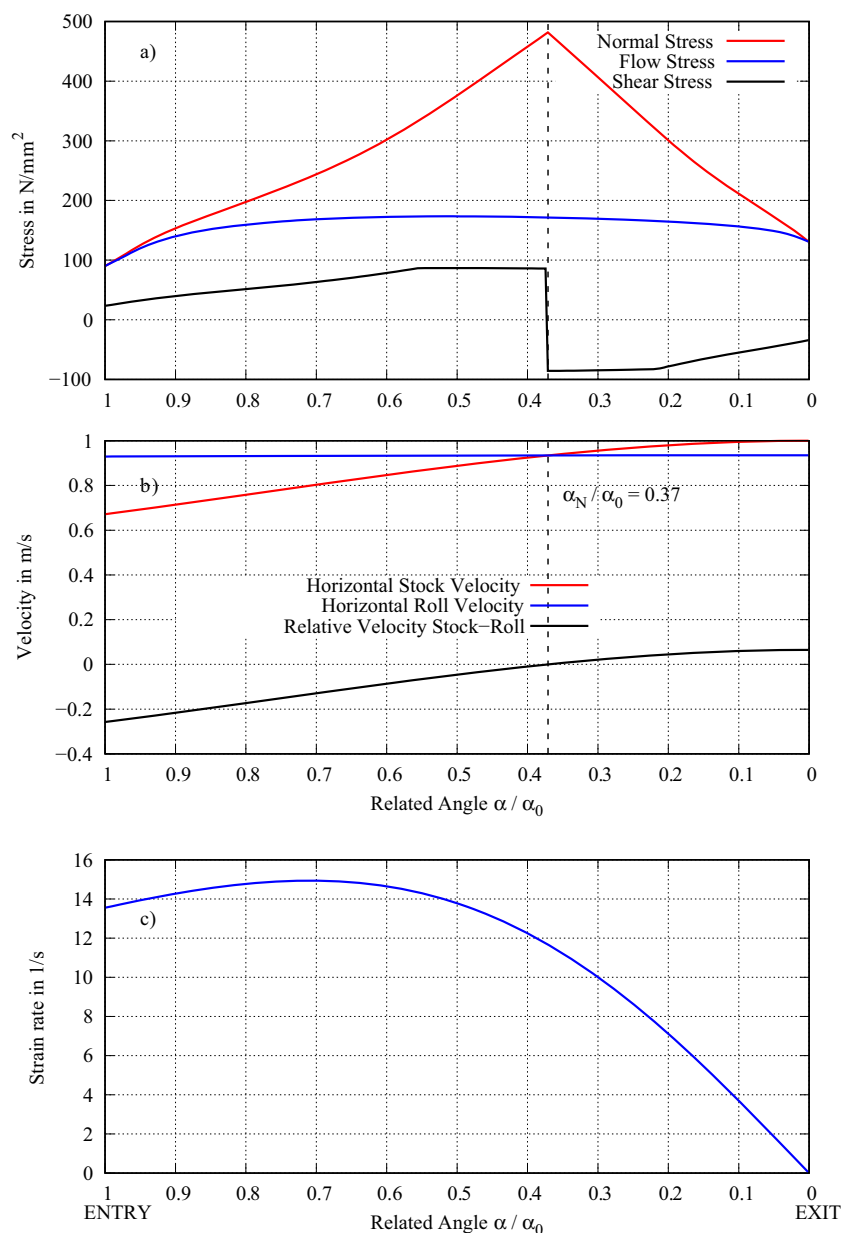
$\Phi(n)$ is the Gauss error function given as:

$$\Phi(n) = \frac{2}{\pi} \int_0^n e^{-t^2} dt \tag{33}$$

In the roll gaps, the deformation energy is nearly completely dissipated as heat. Therefore, a model for the temperature gain due to forming heat generation is:

$$\Delta\vartheta_F = \frac{w_{id}}{c_p(\vartheta)\rho(\vartheta)} \tag{34}$$

The expression w_{id} represents the ideal forming work per unit volume. Generally, it can be defined as the integral of the stress–strain-curve $k_f(\varphi)$ for a specific deformation step:

$$w_{id} = \int_{\varphi_0}^{\varphi_1} k_f d\varphi \tag{35}$$

We may introduce a mean flow stress k_{fm} for the forming step in the roll gap:

$$k_{fm} = \frac{1}{\alpha_0} \int_0^{\alpha_0} k_f(\alpha) d\alpha_0 \tag{36}$$

Note that φ and $\dot\varphi$ vary as a function of α. Generally, $w_{id} = k_{fm}(\varphi_1 - \varphi_0)$. Hence:

$$\Delta\vartheta_F = \frac{k_{fm}(\varphi_1 - \varphi_0)}{c_p(\vartheta)\rho(\vartheta)} \tag{37}$$

Finally, we may calculate the mean roll gap temperature from the arithmetic mean value of the temperatures and the begin and end of the gap:

$$\vartheta_m = \vartheta_0 - \Delta\vartheta_R - \frac{\Delta\vartheta_C - \Delta\vartheta_F}{2} \tag{38}$$

Combining all of the temperature, strain and strain rate effects on the flow stress and implementing the final material model into Alexander's differential equation, we are able to calculate the flow stress, normal stress and shear stress distributions in the roll gap. The differential equation is integrated numerically and the neutral angle is determined from the resulting stress distributions. A typical solution example of the stress, velocity and strain rate distributions is shown in Fig. 2 for a hot rolling pass with the data $h_0 = 10mm$, $h_1 = 6mm$, $R = 300mm$, $v_1 = 1m/s$, $\mu = 0.26$ and the initial temperature $\vartheta_0 = 1000°C$.

Here, it is noteworthy that the flow stress increases after the roll gap entry by strain hardening, until it reaches a maximum and then decreases until the end of the roll gap. This effect is due to the strain rate softening, as the flow stress decreases with decreasing strain rate and the strain rate drops down to zero at the roll gap exit, as shown in Fig. 2c).

The neutral angle found as peak of the normal stress coincides with the sign change in the shear stress distribution. This neutral angle has a related value of $\alpha_N/\alpha_0 = 0.37$ in the example presented. It is equal to the neutral point of the velocity distribution, which is shown in Fig. 2b) and has the meaning of the point where the relative motion between the roll and the stock is zero. We will use this static-kinematic coupling in the roll gap for the purpose of finding the interstand tension, which is described in the following chapter.

2.2 Calculation of interstand tensions in flat rolling

The calculated velocity and stress distributions allow the conclusion that for a given mill setup, the angular velocity ω of the rolls in a single mill stand is influenced by the front and back tensions. The back tension of a mill stand i will now be denoted by $t_{0,i}$, the front tension will be denoted by $t_{1,i}$, respectively.

Figure 3 shows three continuous roll gaps exemplarily. Generally, the front tension of a mill stand i is equivalent to the back tension of stand $i + 1$, i.e. $t_{1,i} = t_{0,i+1}$. For each mill stand i in a continuous arrangement, we can formulate a nonlinear equation relating the back and front tension as well as the volume flux to the angular velocity of the roll:

$$\omega_i = f(t_0, t_1, \dot{V}) \tag{39}$$

For a rolling mill with N mill stands, a system of N nonlinear equations must be solved to find the $N - 1$ unknown tensions t_i and the volume flux $\dot{V}$. It may however be convenient to express the nonlinear system as in Eq. 39 in a linearized form to find a preliminary approximate solution. Assuming linear relationships for the effects of the tensions $t_{0,i}$ and $t_{1,i}$ on the angular velocity ω of the rolls, we can write for a mill stand i:

$$\omega_i = \omega_{0,i} + a_i t_{0,i} + b_i t_{1,i} \tag{40}$$

In Eq. 40, $\omega_{0,i}$ is the designed angular roll velocity for a reference case with zero or moderate tensions. We call this case the reference configuration. The coefficients a_i and b_i are influence parameters for the back and front tensions. We can express this relation for the variation of the angular roll velocity $\Delta\omega_i$ due to variation of the interstand tensions $\Delta t_{0,i}$ and $\Delta t_{1,i}$:

$$\Delta\omega_i = a_i \Delta t_{0,i} + b_i \Delta t_{1,i} \tag{41}$$

Furthermore, we can write for the change of the roll speed difference between two successive mill stands i and $i + 1$:

$$\Delta\omega_{i+1} - \Delta\omega_i = (a_{i+1} - b_i)\, \Delta t_{1,i} - a_i \Delta t_{0,i} + b_{i+1}\Delta t_{1,i+1} \tag{42}$$

Fig. 3 Three roll gaps of a continuous rolling mill

Equation 42 describes the coupling between two successive mill stands due to the acting tensions. Therefore, a system of linear equations can be set up to calculate approximations to the unknown tension differences, which cause the known differences of the roll speeds. It represents the linear equation system with $N - 1$ equations and unknowns, where N is the total number of mill stands in the continuous rolling mill. The back tension of the first stand, was well as the front tension of the last stand is generally treated as zero.

$$\mathbf{A} \mathbf{t} = \mathbf{w} \tag{43}$$

Equation 43 shows the structure of the linear equation system that must be solved for the tensions. The coefficient matrix **A** for N stands is given as:

$$\mathbf{A} = \begin{bmatrix} a_2 - b_1 & b_2 & & & & \\ -a_2 & \ddots & \ddots & & & \\ & \ddots & \ddots & \ddots & & \\ & & -a_i & a_{i+1} - b_i & b_{i+1} & \\ & & & \ddots & \ddots & b_{N-1} \\ & & & & -a_{N-1} & a_N - b_{N-1} \end{bmatrix} \tag{44}$$

The right-hand side vector **w** comprises the changes in the roll speed differences between two subsequent mill stands, relative to the initial reference state:

$$\mathbf{w} = \begin{bmatrix} \Delta\omega_2 - \Delta\omega_1 \\ \vdots \\ \Delta\omega_{i+1} - \Delta\omega_i \\ \vdots \\ \Delta\omega_N - \Delta\omega_{N-1} \end{bmatrix} \tag{45}$$

In Eq. 45, $\Delta\omega_i$ is the change of the angular roll velocity ω_i of mill stand i relative to the original angular velocity of the

reference configuration. The remaining problem is the definition of the influence parameters a_i and b_i for each mill stand i. These are the partial derivatives of the angular velocity with respect to the back and front tension stresses.

With reference to Eq. 40, we write:

$$a_i = \frac{\partial\omega_i}{\partial t_{0,i}} \tag{46}$$

$$b_i = \frac{\partial\omega_i}{\partial t_{1,i}} \tag{47}$$

These differentials can be written as a composite function comprising a kinematic and a static part. We can apply the chain rule to Eqs. 46 and 47 to arrive at the following definitions:

$$a_i = \frac{\partial\omega_i}{\partial t_{0,i}} = \frac{\partial\omega_i}{\partial\alpha_{N,i}} \frac{\partial\alpha_{N,i}}{\partial t_{0,i}} \tag{48}$$

$$b_i = \frac{\partial\omega_i}{\partial t_{1,i}} = \frac{\partial\omega_i}{\partial\alpha_{N,i}} \frac{\partial\alpha_{N,i}}{\partial t_{1,i}} \tag{49}$$

The kinematic derivative $\frac{\partial\omega_i}{\partial\alpha_{N,i}}$ can be worked out by help of the volume flux. For the angular velocity as a function of the neutral angle α_N, we can write with the volume flux $\dot{V}$, the roll radius R and the exit height and width h_1 and b_1:

$$\omega(\alpha_N) = \frac{\dot{V}}{b_1 R \left[h_1 + 2R \left(1 - \cos\alpha_N \right) \right] \cos\alpha_N} \tag{50}$$

Deriving this equation with respect to α_N, we arrive at the final kinematic equation:

$$\frac{\partial\omega}{\partial\alpha_N} = \frac{\dot{V} \sin\alpha_N \left(2R + h_1 - 4R \cos\alpha_N \right)}{b_1 R \cos^2\alpha_N \left(2R + h_1 - 2R \cos\alpha_N \right)^2} \tag{51}$$

The static part comprises two equations describing the influences of the front and back tensions on the neutral angle which can be found from the rolling model. There are rolling

models available which allow a direct calculation of the neutral angle as functions of the front and back tensions, however these models are limited to simplified friction conditions (i.e. pure sticking friction condition along the arc of contact). With Alexander's model, we use a more sophisticated rolling model which requires a numerical solution to find the neutral angle. In this context, a more general treatment of this problem is necessary. We may generally understand the neutral angle as a function of the entry and exit tensions, $\alpha_N = \alpha_N(t_0, t_1)$. The partial derivatives needed by Eqs. 46 and 47 for the calculation of a_i and b_i can then be approximated by the following central difference quotients:

$$\frac{\partial \alpha_N}{\partial t_0} \approx \frac{\alpha_N(t_0 + \Delta_t, t_1) - \alpha_N(t_0 - \Delta_t, t_1)}{2\Delta_t} \tag{52}$$

$$\frac{\partial \alpha_N}{\partial t_1} \approx \frac{\alpha_N(t_0, t_1 + \Delta_t) - \alpha_N(t_0, t_1 - \Delta_t)}{2\Delta_t} \tag{53}$$

Here, Δ_t represents an environment around the working point with the tensions t_0 and t_1 at which the derivatives are to be evaluated. Δ_t must be chosen sufficiently small in order to construct a secant whose slope is evaluated by Eqs. 52 and 53.

With these equations developed, it is now posssible to calculate the interstand tension changes that arise from certain

changes to the mill setup and rolling parameters by a numerical algorithm, which is described in the next section.

2.3 Numerical algorithm of the model

Since the interstand tensions and the volume flux of the rolling process are interdependent, an iterative calculation scheme must be applied. First, we can apply the rolling model to the given pass schedule in order to calculate the angular roll velocities that match a given sequence of interstand tensions, which we call the reference configuration or the design state. Later we will calculate the differences in tension that result from changes to the reference configuration.

This reference configuration is then used to compute the tension influence coefficients a_i and b_i for each mill stand i. Afterwards, the coefficient matrix acc. to Eq. 44 is built using these influence coefficients. To calculate the tension variations arising due to variations of the roll speeds, we can setup the right hand side of Eq. 43 using the known velocity differences. The solution of the linear system then yields a first approximation to the interstand tension deviations in relation to the reference configuration.

As the considered system is non-linear, i.e. the influence coefficients depend upon the tensions, these first approxima-

Fig. 4 Numerical algorithm for the analytical model
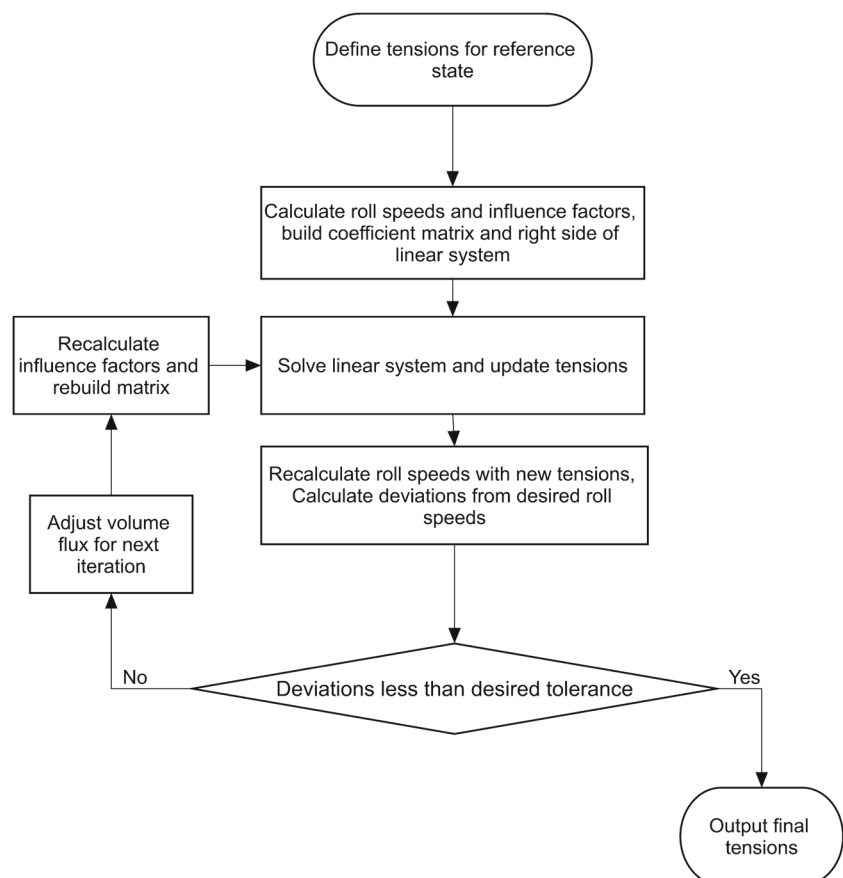
tions of interstand tensions will still lead to angular velocities deviating from the actual ones. For numerical stability, we update the tensions of the reference configuration with the calculated tension deviations with a successive underrelaxation factor f_R:

$$t_i = t_{i,old} + f_R \Delta t_i \tag{54}$$

In Eq. 54, f_R is in the order of magnitude of $f_R \approx 0.5$.

The approximated tensions are used as a new reference configuration and the influence coefficients are recalculated for the next iteration. As Fig. 4 shows, the linear system is solved again for the new reference configuration and the residuals are recalculated.

These steps are repeated iteratively. Before a new iteration is entered, the volume flux is corrected to meet the calculated exit strip velocity of the last stand according to:

$$v = v - b_e h_e R_n (\omega_{0,n} - \omega_n)(1 + \kappa_n) f_R \tag{55}$$

The relaxation factor f_R in Eq. 55 is the same as in Eq. 54. The values h_e, b_e and R_n are the strip thickness, strip width and the roll radius of the final pass, κ_n is the forward slip of the final pass. ω_n is the calculated angular roll velocity of the final pass, $\omega_{0,n}$ is the intended angular roll velocity. The iterative process is repeated until the deviation of the calculated angular velocities from the originally intended ones is smaller than a predefined tolerance value. Additionally, a relative convergence criterion is observed to ensure the calculated tensions in the last 5 iterations do not deviate significantly. After the iterative calculation is finished, the final interstand tensions and the final volume flux have been found and all other rolling parameters can be calculated from the rolling model using these values.

2.4 Tension calculation with spread

If lateral spread of a non-neglible magnitude is present in the rolling process, the calculation of the roll speeds and interstand tensions gains a higher amount of nonlinearity. For rolling tension-free rolling, a number of spread equations are available, which have already been discussed by Mauk and Kopp [17]. Their outcome was that Marini's spread equation [13] provides a precise basis for the calculation of spread under hot rolling of flat products. It considers geometrical features of the rolling process as well as the friction coefficient μ. The calculation of the exit width w_1 is given as:

$$w_1 = w_0 + \frac{2\Delta h w_0 \left(R - \frac{h_0}{2}\right) B}{h_1 w_0 + M_1 + 2h_1 R B} \tag{56}$$

With the definitions:

$$A = \frac{\sqrt{\Delta h}}{2\mu\sqrt{R}} \tag{57}$$

$$B = \sqrt{\frac{\Delta h}{R}} \tag{58}$$

$$M_1 = \frac{w_0(h_0 + h_1)}{2} \cdot \frac{1 + A}{1 - A} \cdot \frac{0.91(w_0 + 3h_0)}{4h_0} \tag{59}$$

From the volume flux in rolling, we can write for the angular roll velocity when we express the rectangular cross sections by the product $A = hw$:

$$\omega = \frac{h_1 w_1 v_1}{R \cos \alpha_N h_N w_N} \tag{60}$$

In Eq. 60, w_N is the width of the rolled material at the neutral plane, $w_N = w(\alpha_N)$. To evaluate this equation, we need to know the width function $w(\alpha)$ in the roll gap. This function can be derived from a locally applied empirical spread model, or better from a plasticity approach of lateral spread. Domanti's asymptotic approach to Hill's General Method [4, 5] is used in the following analysis. The Domanti solution is limited to wide flat sections what concerns the absolute width calculation, but the relative spreading function can be used for all types of rolling processes, when it is scaled to a fixed exit width calculated by a precise empirical spread formula. Therefore, we use a combination of Marini's spread equation [13] and Domanti's asymptotic model as described above. An example for a typical spreading distribution in a roll pass calculated by this method is shown in Fig. 5.
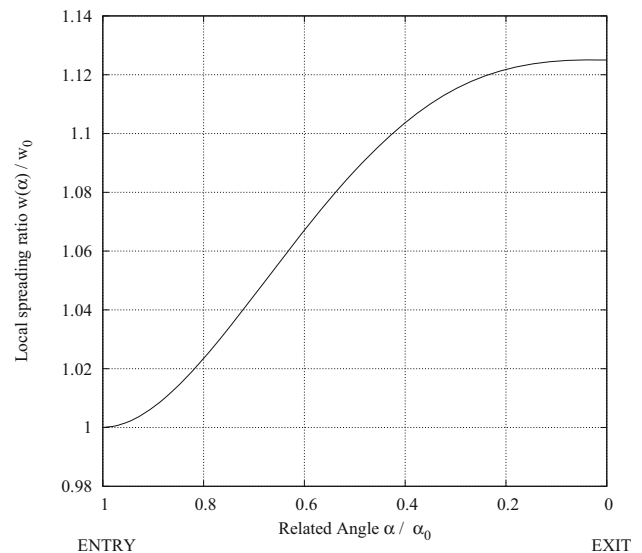

Fig. 5 Domanti's spread function for a rectangular flat pass, entry: 40 mm square, exit height $h_1 = 30$ mm, roll diameter $d = 600$ mm

Table 1 Coefficients for the empirical model for the influence of interstand tensions on lateral spread

i	m_{i1}	m_{i2}	m_{i3}
1	1.05502	0.100816	−0.591029
2	−0.886507	−0.00258613	0.159971
3	−0.347681	−0.457338	0.0525161

The absolute spread also depends on the acting interstand tensions. We may formulate this influence in terms of Mauk's empirical model [14] by stating that the total natural strain φ_A in the pass is given by:

$$\varphi_A = \ln\left(\frac{A_1}{A_0}\right) = \varphi_{A,0} + \Delta\varphi_{A,\sigma} \tag{61}$$

Note that $\varphi_A < 0$ as the cross section is reduced in the roll pass. Now, we may partition the total natural strain φ_A into a contribution assuming maximum spread (disregarding tension effects) $\varphi_{A,0}$, and a tension-influenced strain contribution $\Delta\varphi_{A,\sigma}$. The contribution assuming maximum spread can be calculated from

$$\varphi_{A,0} = \ln\left(\frac{A_1^*}{A_0}\right) \tag{62}$$

In Eq. 62, A_1^* is the exit section of the pass calculated with maximum spread.

The strain contribution which is influenced by the tensions, related to the mean flow stress k_{fm}, is modelled by an empirical equation as a function of the acting tensions and the geometrical parameters:

$$\Delta\varphi_{A,\sigma} = k_1\left(\frac{t_0}{k_{fm}}\right)^2 + k_2\left(\frac{t_0}{k_{fm}}\right) + k_3\left(\frac{t_1}{k_{fm}}\right) \tag{63}$$
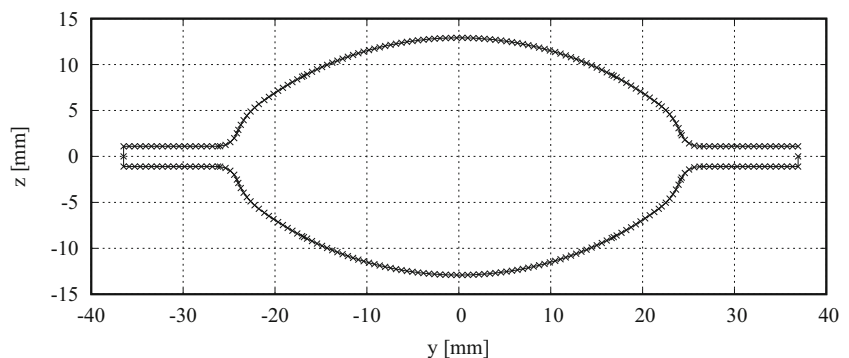
The coefficients k_i in Eq. 63 are functions of the pass geometry:

$$k_i = m_{i1}\frac{\Delta h}{h_0} + m_{i2}\frac{w_0}{h_0} + m_{i3}\frac{A_d}{A_m}, i = 1\dots 3 \tag{64}$$

The coefficients m_{i1} to m_{i3} are found by linear regression of experimental results. Table 1 shows the coefficients which were found by regression analysis of rolling trials with tensions carried out by and Nikkila and Treis [18, 25].

With help of these relations, we can apply the numerical model for the interstand tension prediction as described in Sect. 2.3 to rolling processes with non-negligible spread effects.

2.5 Calculation of section passes in a round-oval-round pass sequence

For rolling processes in wire rod and bar mills, non-cylindrical rolls are used with certain groove geometries to produce the desired product shapes. The calulation of spread and height deformation therefore is more complicated then for rectangular flat sections. Consequently, a rectangular pass method is used to transform the section pass in to an equivalent flat pass. In the present analysis, Lendl's equivalent rectangular pass method is used [12]. The rectangular pass method allows the theoretical concepts of the flat rolling theory to be transfered to section rolling, therefore enabling the interstand tension assessment by the method described before to be applied to section geometries. To enable a numerical treatment of the non-flat geometries, these are described numerically by polygonal contours with small step widths. An example is given for a double-radius oval groove shown in Fig. 6.

By using this approach, arbitraty geometries can be processed. The necessary information is given in the form of vectors of the x and y coordinates. The geometrical operations needed to calculate the equivalent flat pass and the exit section shapes are implemented using the **x** and **y** vectors. Lendl's rectangular pass method allows the construction of

Fig. 6 Geometry of a double-radius oval groove by discrete points as a polygonal contour

Fig. 7 Lendl's method on a pass round to oval. The shaded areas represent the equivalent areas A_{0L} and A_{1L}
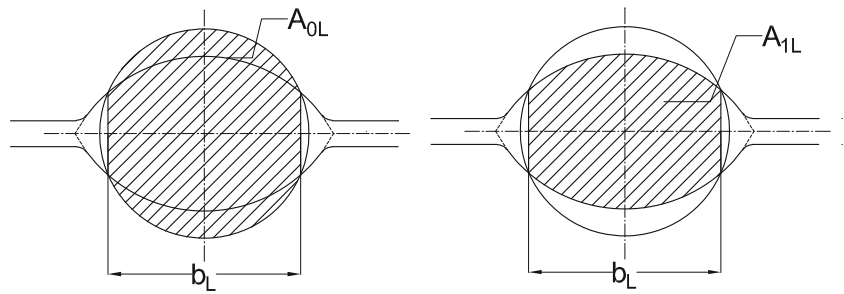
an equivalent flat pass by using the equivalence areas A_{0L} and A_{1L}. These are shown exemplarily for a pass round to oval in Fig. 7.

The equivalent mean heights for the rectangular flat pass are then calculated from:

$$h_{0L} = \frac{A_{0L}}{b_L} \tag{65}$$

$$h_{1L} = \frac{A_{1L}}{b_L} \tag{66}$$

In these equations, b_L is the intersection distance of the initial and groove contours as shown in Fig. 7. We define a working roll diameter d_{wrk} in the following way using the nominal barrel diameter of the roll d_N:

$$d_{wrk} = d_N - h_{1L} + s \tag{67}$$

The spread calculation for the oval pass can then be carried out with the data h_{0L}, h_{1L}, d_{wrk} and using the initial section width $w_0 = d_0$ of the entry round section. In the present model, we use Marini's spread equation as given by Eq. 56 for this purpose.

We can understand why the lateral spread is of essential importance for hot rolled long products by looking at Fig. 8.
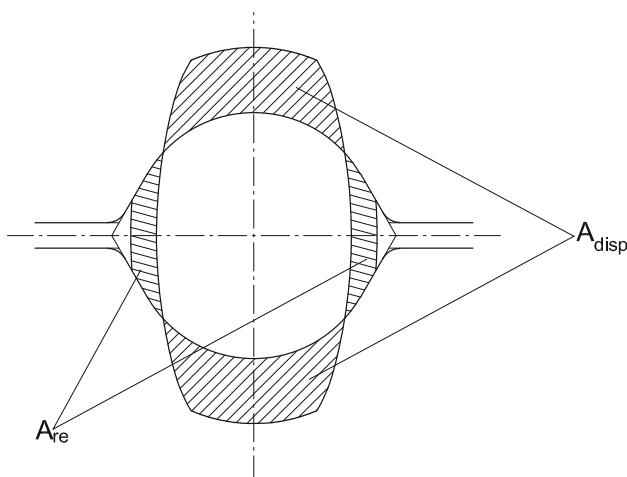
Fig. 8 Displaced area A_{disp} and reappearing area A_{re} at the pass oval to round

It shows the height and width deformations on a pass oval to round.

It is seen that parts of the original cross section are displaced by the rolls (the displaced surface A_{disp}). A part of this displaced surface reappears by lateral spread as the reappearing surface A_{re}. The relation of these two surface parts is measured by the elongation efficiency f_S:

$$f_S = 1 - \frac{A_{re}}{A_{disp}} \tag{68}$$

We should note that A_{disp} is the result of lateral spread in the preceding pass. Therefore, we can save deformation energy by keeping the elongation efficiency at a high level. As seen by Eq. 68, f_S is high when the spread is low. Under optimal circumstances, one or more stands of a mill could be saved when smaller roll diameters are used, which effectively reduce the lateral spread and thereforce increase the elongation efficiency [15]. Also, interstand tensions can help in improving the elongation efficiency. Therefore, examples for the assessment of interstand tensions in long product rolling are shown in the next sections.

2.6 The effect of mill spring and interstand tensions on the section geometry of round products

In the case of long products, it is essential to consider elastic rolling stands. We should recall that most rolling mills for long products, which are in operation nowadays do neither have an automatic gagemeter control, nor hydraulic screw-down components which would allow for roll gap corrections under load.

To assess the effects of interstand tensions on the section shape we use the empirical model described in section 2.4. An example for the results in a round pass is shown in Fig. 9.

The first case (left part of Fig. 9) represents the reference case free from tensions and disregarding any mill spring, as for a mill stand with an infinite rigidity. Here, a designed groove height of 12.41 mm is met at a section width of 12.83 mm, yielding a roll force of 83.8 kN. In the more practical case of an elastic mill stand (see right part of Fig. 9) with a rigidity constant of 350 kN/mm, back and front tensions of 29.9 MPa and 56.3 MPa are encountered. These tensions

Fig. 9 Calculated influence of interstand tensions and elastic mill spring on the rolled cross section in a round-oval-round pass sequence

rigid stand
no tensions
roll force: 83.8 kN
mean yield stress: 229 N/mm²

elastic stand, rigidity: 350 kN/mm
roll force: 63.5 kN
back tension: 29.9 N/mm²
front tension: 56.3 N/mm²
mean yield stress: 223 N/mm²
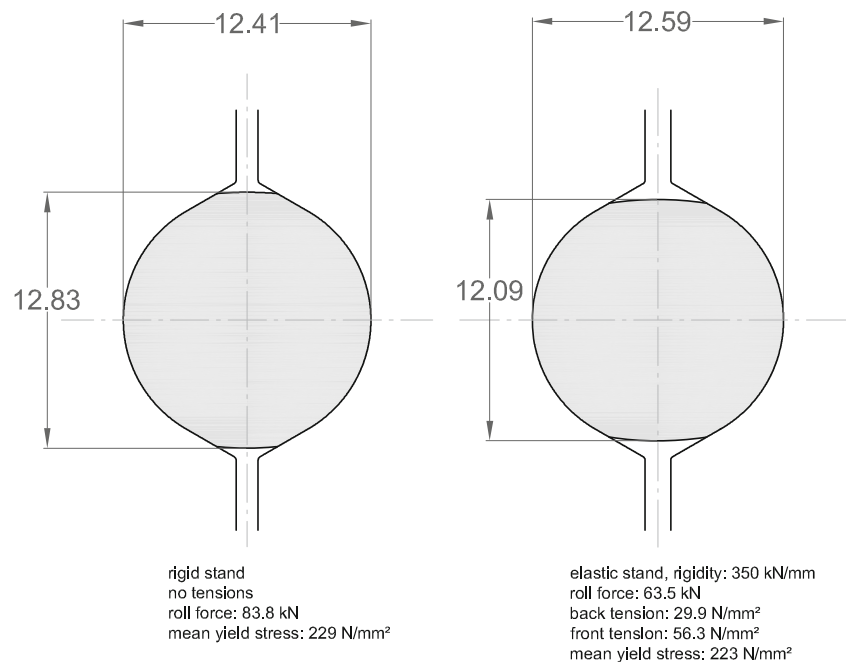
induce a roll force decrease to 63.5 kN. Since the stand behaves elastically, the roll force leads to a mill spring that produces an exit height of 12.59 mm. The tensions decrease the lateral spread to a final width of 12.09 kN. Note that the interacting effects of the temperature distribution and subsequent section changes are treated accordingly by the overall model. Therefore, the coupling of the different mill stands due to mill spring and the tensions are taken into account.

3 Results of the model for industrial rolling processes

In this section, numerical results of the model discussed before are presented for a number of industrial rolling processes, starting with a typical pass schedule for a finishing train of a wide hot strip mill, where the effects of initial thickness, temperature and friction are shown in detail. In this rolling process with a high width-to-thickness relation of $w/h > 25$, lateral spread can be disregarded, so the principal influences without spread are shown. The next example concerns a flat rolling process with a noticeable amount of spread, starting from a square section of 50x50 mm. The last set of examples comprises long product rolling cases for round wire rod and bars, where the typical influences of varying entry sections on the interstand tension distribution is shown.

3.1 Material Coefficients of the Hot Flow Curve

For all computations presented in this section, a mild carbon steel with 0.55 weight percent of carbon was chosen (AISI

1055 / DIN 1.0535). The hot flow curve equation used is given by Eq. 24. The material-dependent coefficients in the equation were found by a linear regression analysis for experimental data given by Cook [3], who used high-temperature compression tests to gather the data. The regression analysis was carried out using the fitlm subroutine of MATLAB R2021b. The resultant coefficients along with the ranges of the experimental data are given in Table 2. The determination constant achieved with Eq. 24 was $R^2 = 0.994$.

3.2 Finishing train of a hot strip mill

First, a seven-stand finishing train of a hot strip mill will be considered, which is designed to work with moderate tensions of 20 MPa between the stands. A transfer bar with an

Table 2 Coefficients and experimental data range of the how flow curve used for the material AISI 1055

Figure	Value	Unit
k_0	4558.87	MPa
m_1	−0.0032118	-
m_2	−0.0399528	-
m_3	0.2591754	-
m_4	−0.5906081	-
m_5	0.0001778	-
R^2	0.994	-
$\dot{\varphi}$	0.5 . . . 100	s^{-1}
ϑ	900 . . . 1200	°C
φ	0.05 . . . 0.7	-

Table 3 Pass Schedule of an industrial hot strip mill finishing train. h_1: Strip Thickness; d_R: Roll Diameter; t_1: Front Tension; w_1: Strip Width

Pass	h_1 in mm	d_R in mm	t_1 in MPa	w_1 in mm
Initial	40.00			1000.00
1	26.42	600	20	1002.63
2	17.74	600	20	1004.21
3	12.05	600	20	1005.15
4	8.33	600	20	1005.68
5	5.84	600	20	1005.99
6	4.15	600	20	1006.17
7	3.00	600	0	1006.27

initial thickness of $h_0 = 40$ mm is reduced to a final strip thickness of $h_7 = 3.0$ mm at a finished rolling speed of $v_e = 10$ m/s out of the last mill stand. The pass schedule is given in Table 3.

Different authors argue that the lateral spread is insignificant for the high width-to-height relations present in the finishing train of a wide hot strip mill [9–11, 22]. Yu carried out an experimental analysis by preparing a slab of 129 mm thickness and 2465 mm width with multiple rows of pinholes to measure the lateral displacements [27]. Yu came to the conclusion that the total width variation was in no case more than 7 mm, but there were remarkable lateral flow effects between the center and edge segments of the strip. However, for the present study, the total width variation is of greater interest than the local transverse material flow. Therefore, the exit strip widths of each pass were calculated according to Marini's spread model given in Eq. 56. The results are presented in Table 3. It is seen that the width variations are very low compared to the total strip width, so the strip rolling process was treated as plane-strain for this specific example.

In this example, we disregard elastic mill spring, since it is state-of-the-art for wide hot strip mills to work with automatic gage controls (AGC) where roll force variations are directly compensated by hydraulic screw-down adjustments. The resulting elastic stiffnesses of such stands would therefore be extremely high, resulting in negligible mill spring.

3.2.1 Influence of a transfer bar height variation on interstand tensions

It is known from rolling mill practice, that the height of the transfer bar entering the finishing train influences the interstand tension distribution. This effect can be calculated using the present model. Figure 10 shows the calculated tension distribution for the finishing train, if the tranfer bar thickness is varied up to ±10% of the reference height of 40 mm.

The reference case returns the originally given tensions of 20 MPa. If the strip entry thickness is reduced by 10 %,
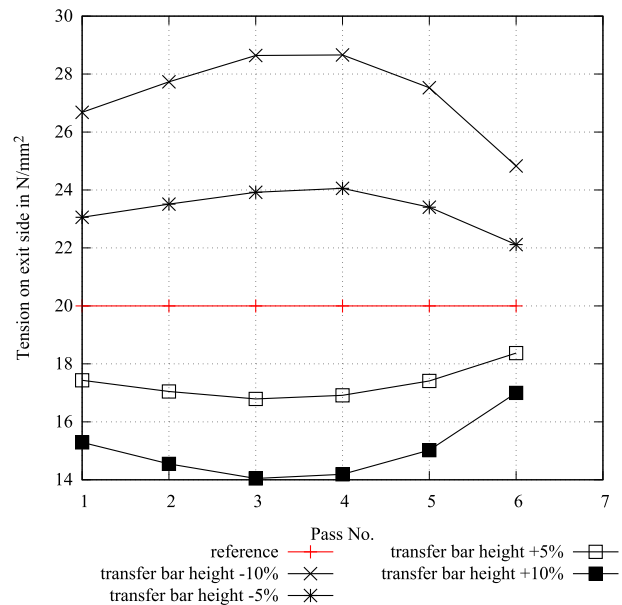

Fig. 10 Calculated influence of varying transfer bar thickness on the tension behaviour of the finishing train

the tensions rise to values ranging from 26.5 MPa to a maximum value of 28.5 MPa. In the opposite case, if the entry thickness is increased by 10 percent, the interstand tensions in the finishing train decrease to values between 14 MPa and 17 MPa.

3.2.2 Friction influence on the interstand tension distribution

The interstand tension distribution is expected to vary with the present friction conditions. To examine this effect, the reference case with constant tensions of 20 MPa and a friction coefficient of $\mu = 0.3$ is compared to cases of a varied friction coefficient between $\mu_{min} = 0.25$ and $\mu_{max} = 0.35$. The numerical results of this study are shown in Fig. 11.

It can be seen that in the considered cases, a decreasing coefficient of friction leads to increasing interstand tensions. Generally, it can be stated that the friction coefficient does have a high impact on the tension distribution in a continuous rolling mill, as Fig. 11 shows. For the operational practice of a continuous rolling mill, interstand tensions have to be expected to vary extensively with the present friction conditions.

3.2.3 The influence of the rolling temperature on interstand tensions

Another effect on the tension distribution to be examined is that of the rolling temperature. Figure 12 shows the tension distributions which result from varied entry temperatures in
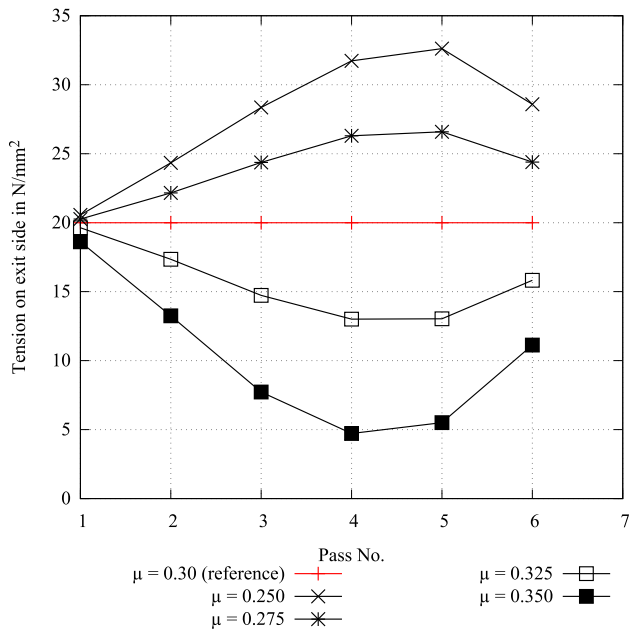
Fig. 11 Calculated influence of friction on the tension behaviour of the finishing train

the finishing train. It is seen that the calculated interstand tensions increase with decreasing rolling temperature.

3.3 Flat rolling with lateral spread

Applying the Equations given in Sect. 2.4, we can directly calculate the angular roll velocities for a given set of
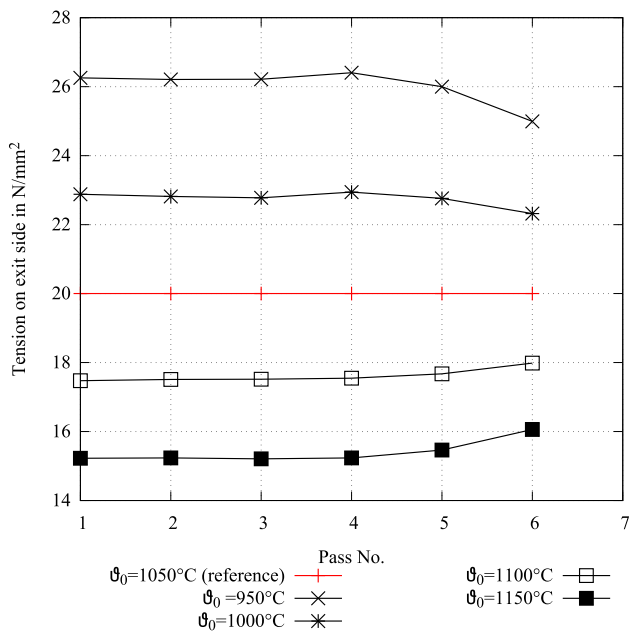
interstand tensions, taking into account the lateral spread affected by the tension influence. It is important to note that the resulting tension influence on the designed angular roll velocities originates from two different effects, the first being the direct influence of the tensions on the shift of the neutral point, the second originating from a distortion of the volume flux, when the spreading and therefore the rolled cross sections are affected by the tensions.

Figure 13 shows a comparison of the designed roll velocities for the same pass schedule under lateral spread, starting with a 50x50 mm square section, rolled down continuously to a final height of $h_e = 20mm$. In the Figure, the black curves with the plus and cross markers show the case where the tension-dependency of the lateral spread is disregarded and the tension effects are controlled by the neutral point shift only. These examples are marked with s in the legend. The red curves with the box and circle markers show the calculations with the tension-influenced spread taken into account, marked with c in the legend. We can observe that the differences between the curves of the first set are very small compared to the second set. Therefore, we can conclude that the effect of the neutral point shift on the angular roll velocities is small compared to the combined neutral point shift and volume flux effects, which are controlled by the reduced lateral spread due to the interstand tensions.

Figure 14 shows the resulting section widths for the parameter combinations considered in Fig. 13. The interstand tension leads to a significant decrease of the section widths, which shows effects on the calculated angular roll velocities.
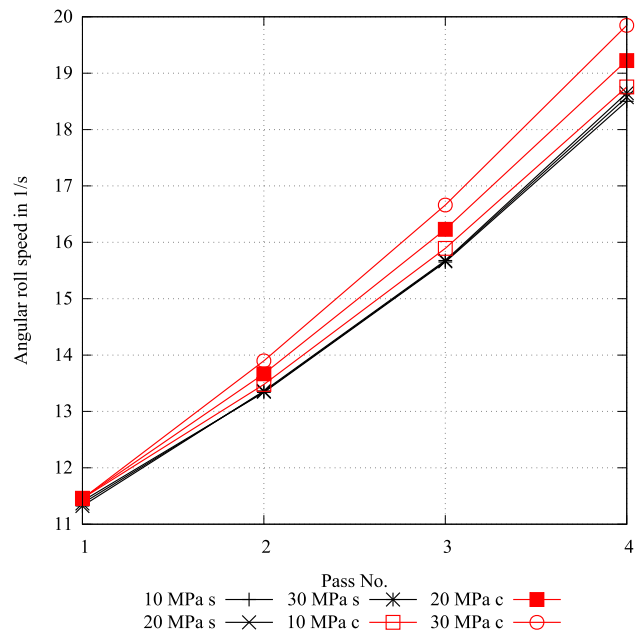

Fig. 12 Calculated influence of entry temperature on the tension behaviour of the finishing train

Fig. 13 Influence of the interstand tensions on calculated angular roll velocities. s: tension-influence on spread disregarded; c: tension-influence on spread accounted for
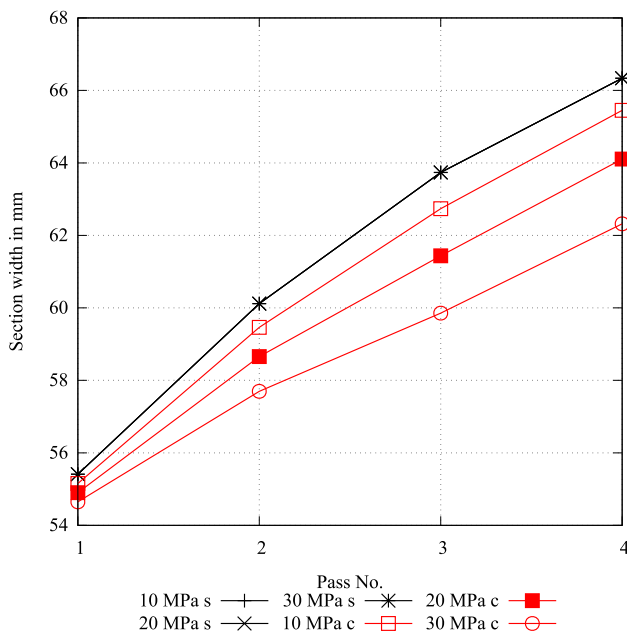
Fig. 14 Influence of the interstand tensions on calculated section widths

The inverse calculation of the acting tensions as described in the preceding sections can be carried out in a similar way. Figure 15 shows calculated examples. The black curves represent the interstand tensions in the four-stand mill with the tension influence on lateral spread disregarded. The influence of the entry thickness on the resulting tensions is very high. For the cases with the tension-effects taken in to account
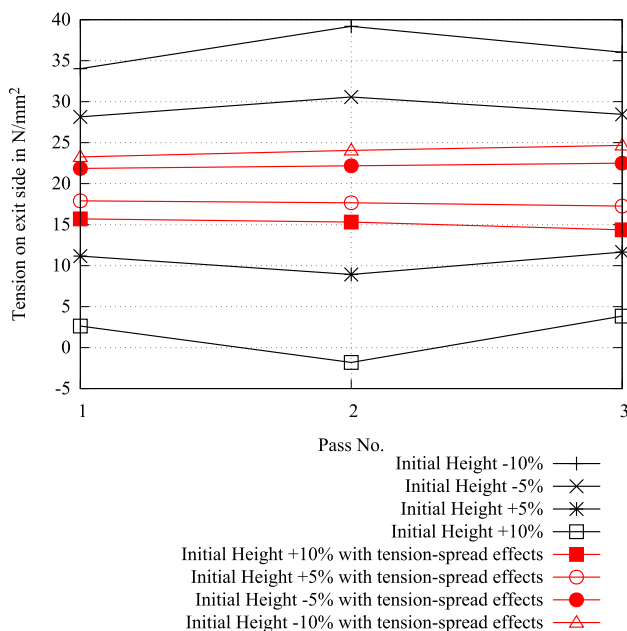
Fig. 15 Comparison of calculated interstand tension distributions with and without tension-influenced spreading effects

represented by the red curves, the overall tension influence is much lower.

3.4 Calculated examples for an industrial single-strand wire rod mill

For the inverse tension calculation in a wire rod mill, the present model can be used in a way similar to the method presented for flat product rolling. Here, the second intermediate mill of a single-strand wire rod mill will be treated. The roll pass design of this six-stand mill arrangement is shown in Fig. 16. An initial round section with a nominal diameter of 32 mm is reduced to a final section of 15.5 mm in diameter, which serves as the entry section to the wire rod finishing block.

First, the angular velocities of the rolls were designed for a reference configuration with moderate interstand tensions of 10 % of the flow stress. This specific value was chosen to incorporate a safety against buckling of the rolled stock, when the tensions would be reduced by process variations.

With the same angular roll velocities, a parameter study was carried out to examine the influence of a varying entry section on the resulting interstand tensions.

Figure 17 shows the calculated tensions distributions for a 32 mm entry (nominal) and two varied entry cross sections of 31.5 mm and 32.5 mm.

From the calculated results we can see that for the bigger entry section, the interstand tension drops and is reduced to a near to zero tension between the last two passes. On the other hand, when the entry section is decresed to 31.5 mm, interstand tension rise to higher values. In Fig. 18 we can see how the deformation process reacts to these changed interstand tensions.

For the reference condition, a close to round exit section is obtained with 15.5 mm in height and 15.6 mm in width direction. When the entry section decreases to 31.5 mm, higher tensions are generated. For the final pass, the back tension increases from 21 mm to 37 mm, see Fig. 17. The increase of the interstand tensions between all passes results in a significant decrease of the lateral spread in all passes. For this case, a final section with a width of only 15 mm is generated to serve as the starting section for the finishing block. In the opposite case, when the entry section is enlarged to 32.5 mm, the tensions are significantly decreased and the lateral spread will increase (relative to the reference configuration), resulting in an already overfilled round section with a width of 16.4 mm (see Fig. 18). Note that the angular roll velocities remain constant for all three cases considered, so the calculation results indicate what deviations of the final sections have to be expected when the initial section undergoes the discussed variations under operation.

To enable a non-faulty rolling process for the 32.5 mm initial section, the roll velocities must be adjusted by forward-

Fig. 16 Pass design of the second intermediate mill of a single-strand wire rod mill for the smallest final section
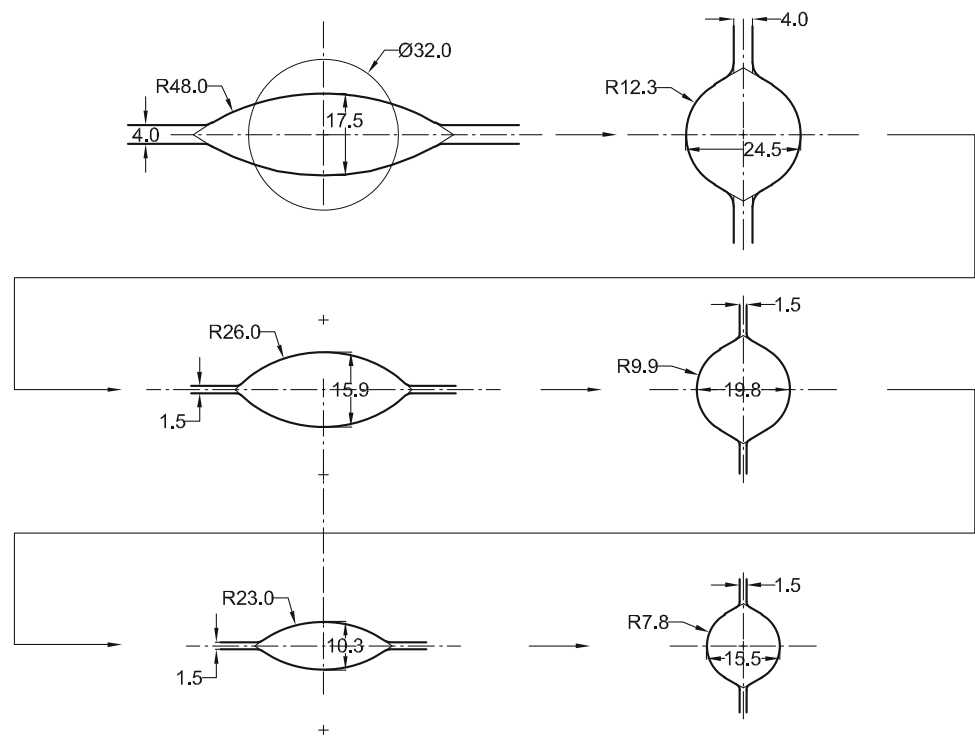
evaluation of the model. Table 4 shows the original and optimized angular roll velocities and interstand tensions.

The variations of the nominal 15.5 mm entry to the finishing block will also affect the rolling process in the finishing block in a similar way as discussed for the intermediate mill. In the finishing block of a wire rod mill, the final rolling speed for the smallest section can be up to 120 m/s. These high rolling speeds are necessary to utilize the production capacity of the rolling mill as far as possible and therefore enable an economic production. The vast majority of today's wire rod mills utilize 10-stand finishing blocks with a fixed

gear system and a common drive for all stands. In this situation, the rotational speeds of all rolls remain in a fixed relation and it is not possible to control the interstand tensions during operation by changing the rotational speed of one stand relative to the other ones. Because of this fact, the wire rod finishing block is an interesting industrial example to be studied using the new tension calculation model.

Figure 19 shows the pass design of the ten-stand finishing block for the nominal output section of 5.0 mm with details of the groove geometries given in Table 5.

In a parametric study, the initial round section of the finishing block was varied between 15.0 mm and 15.7 mm, where the nominal design condition is a 15.5 mm round section.

Figure 20 shows the interstand tension distributions that are encountered for the different conditions.

The typical shape of these distributions follows from the mill spring which is strongly connected to the reduction distribution of the finishing block, featuring higher reductions in the oval passes than in the round passes, and as a conclusion higher roll forces and mill spring. For the smallest entry section considered (15.0 mm), very high tensions of up to 81 MPa are encountered, where for the biggest entry section of 15.7 mm, the tensions are decreased very much with a small compression stress between the first two passes.

Figure 21 shows the final sections which must be expected for the different entry section conditions, where the back tensions for the final pass are given in Table 6.

Generally, we can observe that the height of the final section is not severely affected by the entry section, as the tension
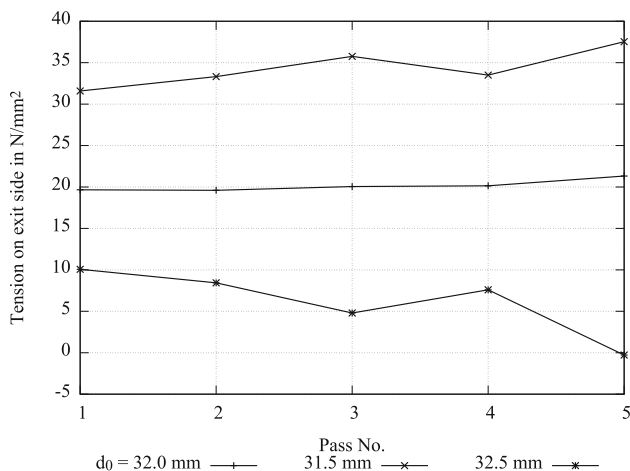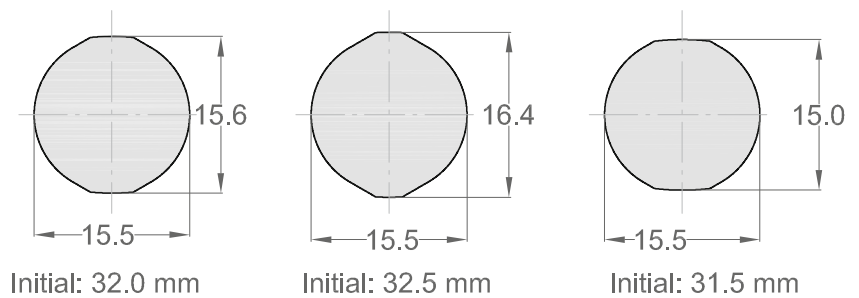

Fig. 17 Calculated interstand tension distribution in the Intermediate Mill 2 for varied entry sections

Fig. 18 Calculated exit section running out of the second intermediate mill for a ± 0.5 mm variation in the entry section

variation generates force and therefore mill spring variations of the final pass when the screw-down remains fixed. In contrast, the section width, being controlled by the acting tension directly, varies between 4.62 mm for the 15 mm entry section up to 5.18 mm for the 15.7 mm entry section.

4 Discussion

In the present paper, a computational model for the inverse calculation of interstand tensions in continuous rolling mills was introduced. The model uses iterative calculations with a rolling model and a linearization of tension-roll velocity relationship. This relationship is formulated internally as a composite function with the neutral angle of the roll gap as central coupling parameter between statics and kinematics.

For the simplest case of negligible lateral spread, calculations for a seven-stand finishing train of a hot strip mill were carried out. It is seen that the interstand tensions depend significantly on the entry height of the transfer bar and on the friction coefficient which is used for the calculation. A temperature influence of the interstand tensions can also be observed using the model, but it should be understood that the effect observed here is mainly controlled by the temperature-dependency of the material's flow curve. The true temperature dependency observed in rolling mill practice will be a combined effect of flow stress and a temperature dependent friction coefficient.

Table 4 Model-based optimizaion of angular roll velocities. ω: original angular roll velocity; ω^*: optimized angular roll velocity

Pass	ω in s^{-1}	ω^* in in s^{-1}	$t_{i,1}$ in MPa	$t_{i,1}^*$ in MPa
1	28.20	27.48	10.07	25.9
2	37.31	37.28	8.43	25.7
3	64.90	65.03	4.79	25.9
4	81.12	81.77	7.60	25.8
5	97.15	97.51	−0.28	27.4
6	128.08	128.56	0.0	0.0

In the next step, the model was applied to a flat rolling pass schedule with apparent lateral spread. An empirical model is used to describe the influence of the tensions upon the lateral spread, an effect which leads to extra nonlinearities in the developed numerical model. It is therefore necessary to introduce a relaxation factor into the model as to ensure a stable convergence. In this study, it was shown that the way in which the roll speed deviations are influenced by interstand tensions is different if the direct spreading-effect of the tensions is taken into account. Therefore, it can be concluded that the static-kinematic relationship in the roll gap is influenced by two effects, the first one being the neutral point shift, the second one being direct distortions of the volume flux. In this interaction, the volume flux plays a major role for practical rolling cases with apparent lateral spread.

The results of the further studies indicate that interstand tensions are of great importance also in rolling mills for long products. To show the principal effects, another study was carried out for a single-strand wire rod mill, where the influence of varying entry sections into the intermediate mill and the finishing block are discussed. In the intermediate mill, the tensions and section formations depend largely on the entry section. It was shown that not only a too big entry section may lead to overspreading in the last passes, but also to very small tensions. Even compressive stresses may be observed, which can lead to mill cobbles and must be avoided. This effect can be counteracted by active steering of the angular roll velocities to ensure higher tensions. For the wire rod finishing block, the model calculations revealed that a precise sizing of the entry section is important to avoid excessive variations in the interstand tensions encountered, as an active control of the angular roll speeds is impossible due to the fixed gear system of the finishing block.

It may be concluded that interstand tensions are a principal influence parameter for rolling processes in continuous rolling mills and therefore must be observed and controlled carefully. In rolling of long products, they play a major role on the achievable product tolerances, since the rolled cross sections can be effectively controlled by a targeted adjustment of the tensions.

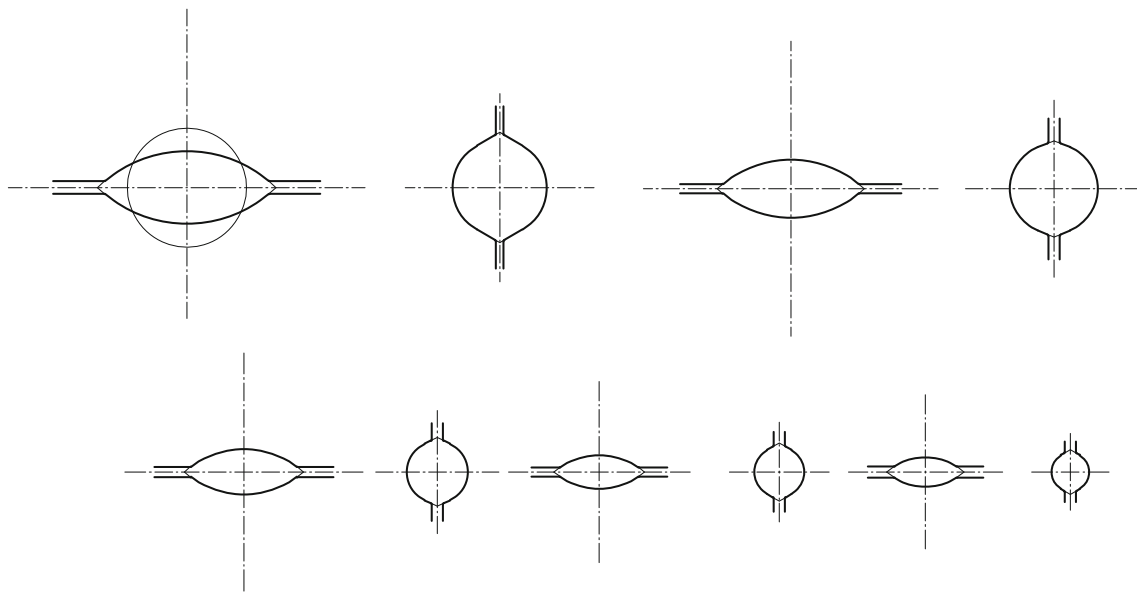As a significant influence of friction on the interstand tension was shown, it is important to develop a method

Fig. 19 Pass design of a ten-stand wire rod finishing block for a 5.0 mm rod out of a nominal 15.5 mm initial section

for a reliable online-measurement of the coefficient of friction during hot rolling in the near future. These methods should be based on optical measurements of the forward slip and section formation, as not to disturb the rolling process. Also, the various influences of the coefficient of friction on temperature, rolling velocity and material pairing (rolls and workpiece) should be worked out using an inline-measurement method to form a better theoretical basis for the description of the friction influence on the lateral spread and side formation.

Another factor influencing the interstand tension distribution is the roll wear. The results of the present work indicate that interstand tensions vary with the friction coefficient substantially. Panjkovic gives a literature review on the change

of the friction coefficient with increasing roll wear [20]. When large pores of an area greater than 0.25 mm^2 (called comet tails) as surface defects develop on the roll surface, a remarkable increase of the coefficient of friction can be expected [26]. Therefore, a reaction of the interstand tensions to increasing surface degradation by wear mechanisms is to be expected.

Secondly, the groove or roll gap shapes change due wear of the roll surfaces. From the studies about the effect of varying

Table 5 Groove data for the 10-stand finishing block

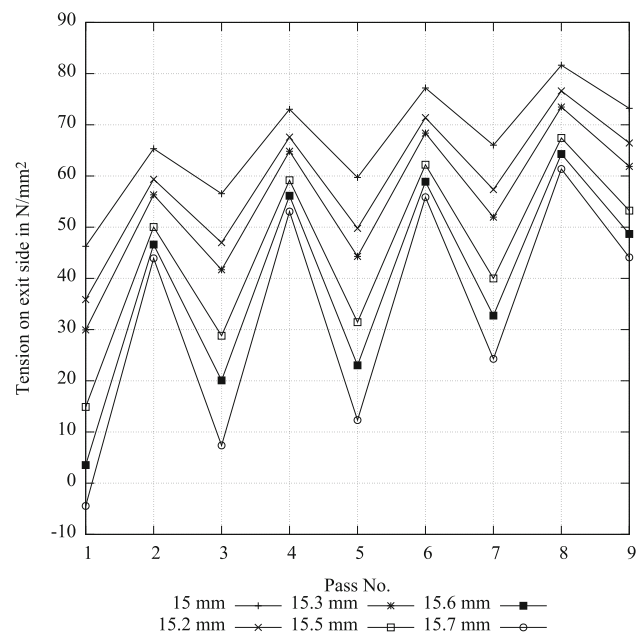| Pass	Type	Height in mm	Radius in mm	Roll Gap in mm
Initial	Section	15.5	7.75	
1	Oval	9.5	16.5	1.6
2	Round	12.24	6.3	0.94
3	Oval	7.6	14.0	1.2
4	Round	10.0	5.1	1.3
5	Oval	6.0	11.5	1.3
6	Round	8.0	4.08	1.5
7	Oval	4.40	9.0	1.2
8	Round	6.50	3.31	1.5
9	Oval	3.85	7.5	1.45
10	Round	5.00	2.55	1.4

Fig. 20 Interstand tension distribution in a 10-stand wire rod finishing block

Fig. 21 Calculated final sections of the 5 mm wire rod as a function of the entry diameter to the finishing block
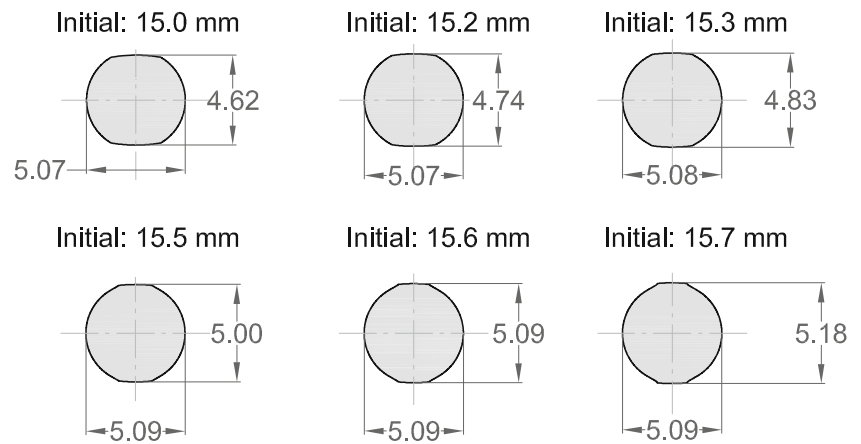
entry sections on the interstand tension distribution included in the present paper, we can conclude that variations of the groove heights in subsequent passes influence the tension distribution to a great extent. This also applies to roll gap or groove shape changes induced by increasing roll wear.

When a worn out roll surface is redressed, the nominal diameter of the roll decreases with effects on the kinematics of the rolling process. The model proposed in the current paper can help to redesign the rotational roll speeds and to predict the interstand tensions to be expected when a roll is subjected to substantial wear.

It would be necessary to conduct further studies to examine the effects of roll wear on the tension distributions, based on the model present in the current paper. A study on online prediction of roll wear in bar rolling mills using an artificial neural network can be found in [23]. A combination of such data-driven wear prediction model with the model presented in the current work would extend the application range of the tension assessment to the cases with substantial roll wear and should be addressed as a future research work.

Finally, we may conclude that the future developments of data-driven modeling and control techniques for rolling mills will require a precise and fast tension calculation model. The present work aims at contributing to a path towards this goal.

Table 6 Metal forming data for the exit sections given in Fig. 21

Entry Diameter in mm	Back Tension in MPa	Height in mm	Width in mm
15.0	73.2	5.07	4.62
15.2	66.5	5.07	4.74
15.3	61.9	5.08	4.83
15.5 (nom.)	53.2	5.09	5.00
15.6	48.7	5.09	5.09
15.7	44.1	5.09	5.18

Author Contributions Christian Overhagen developed the theoretical model, wrote all the software for this work, carried out the calculations including evaluation and wrote this paper.

Data Availibility Statement The calculated data is available on the following Mendeley Data Repository: https://data.mendeley.com/datasets/n7g339nybb/1.

Code Availability The MATLAB code of the flat rolling model is available on the following Mendeley Data Repository: https://data.mendeley.com/datasets/n7g339nybb/1.

Declarations

Conflicts of interest There are no conflicts of interest to declare.

Ethical standard The material included in this paper is original The author wrote all software that was used to generated the calculated results. Neither humans nor animals were involved in this research. The research is part of the author's professional activities, and there is no conflict of interest with any third party.

Consent to participate The author consents to participate in the following process.

Consent for publication The author gives all the rights to publish the material presented in this work.

References

1. Alexander JM (1972) On the theory of rolling. Proc R Soc 326(1567):535–563. https://doi.org/10.1098/rspa.1972.0025

2. Chen S, Li W, Liu X (2014) Calculation of rolling pressure distribution and force based on improved karman equation for hot strip mill. Int J Mech Sci 89:256–263. https://doi.org/10.1016/j.ijmecsci.2014.09.011

3. Cook PM (1957) True stress-strain curves for steel in compression at high temperatures and strain rates for application to the calculation of load and torque in hot rolling. In: Proc. Conference on the properties of materials at high rates of strain. Oxford, 86–97

4. Domanti S, McElwain DLS, Middleton RH (1995) Asymptotic approach to the hill model of spread in rolling. J Eng Mat Technol 117(1):75. https://doi.org/10.1115/1.2804374

5. Hill R (1963) A general method of analysis for metal-working processes. J Mech Phys Sol 11(5):305–326. https://doi.org/10.1016/0022-5096(63)90033-4

6. Hitchcock JH (1935) Roll neck bearings. Report of ASME Special Research Committee on Heavy-duty Anti-friction Bearings, 33–41

7. von Karman T (1925) Beitrag zur theorie des walzvorgangs. Z Angew Math Mech 5:139–141

8. Krzyzanowski M, Beynon JH, Farrugia DCJ (2010) Oxide scale behavior in high temperature metal processing. Wiley-VCH, Weinheim

9. Lal GK, Dixit PM, Venkata Reddy N (2011) Modelling Techniques for Metal Forming Processes. Alpha Science International Ltd., Oxford

10. Lange K (ed) (1985) Handbook of Metal Forming. Mc Graw-Hill Book Company, New York

11. Larke EC (1957) The Rolling of Strip. Sheet and Plate. Chapman and Hall Ltd., London

12. Lendl AE (1948) Rolled bars - part 1 - calculation of spread between non parallel roll surfaces. Iron and Steel 21(14):397–402

13. Marini N (1941) Nuova teoria sulla laminazione. La Metallurgia Italiana, 292–309

14. Mauk PJ (1999) Analysis of interacting influence parameters on the tolerances of wire rod and bars in the rolling process. In: Proceedings of the 6th ICTP International Conference on the Technology of Plasticity, Nuremberg, 1529–1536

15. Mauk PJ (2000) Technical feasibility of using small diameter rolls for hot rolling of bars and wire rod. Der Kalibreur (The Roll Pass Designer) 61(61):49–62

16. Mauk PJ, Gottschling J (2000) Hot flow curves of metallic materials. In: Proceedings of the 14th International Forgemasters Meeting, Wiesbaden, 484–492

17. Mauk PJ, Kopp R (1982) Spread under hot rolling. Der Kalibreur (The Roll Pass Designer) 37(39):3–68

18. Nikkilä K (1977) On the effects of front and back tensions on wire rod rolling. Phd thesis, Helsinki University of Technology, Helsinki

19. Orowan E (1943) The calculation of roll pressure in hot and cold flat rolling. Proc Inst Mech Eng 150:140–167

20. Panjkovic V (2014) Friction and the Hot Rolling of Steel. CRC Press, Boca Raton

21. Pawelski O (1969) Berechnung der wärmedurchgangszahl für das warmwalzen und schmieden. Arch Eisenhüttenwes 40(10):821–827

22. Roberts WL (1983) Hot Rolling of Steel. Marcel Dekker Inc, New York

23. Shigaki Y, Cunha MA (2014) Online prediction of wear on rolls of a bar rolling mill based on semi-analytical equations and artificial neural networks. In: Snasel V, Krömer P, Köppen M, et al (eds) Soft Computing in Industrial Applications, Advances in Intelligent Systems and Computing, 223. Springer, Cham, 243–253, https://doi.org/10.1007/978-3-319-00930-8_22

24. Spuzic S, Narayanan R, Kovacic Z et al (2017) Roll pass design optimisation. Int J Adv Manuf Technol 91(1–4):999–1005. https://doi.org/10.1007/s00170-016-9424-4

25. Treis H (1968) Ermittlung der formänderungsverhältnisse beim warmwalzen auf der flachbahn ohne und mit äußerem längszug. Phd thesis, RWTH Aachen, Aachen

26. Uijtdebroeks H, Franssen R, Franssen G et al (1998) On-line analysis of the work roll surface deterioration in a hot strip mill. Rev Met Paris 95(6):789–800. https://doi.org/10.1051/metal/199895060789

27. Yu Q (2009) Width variation behavior during hot rolling. In: Ginzburg VB (ed) Flat-Rolled Steel Processes - Advanced Technologies. CRC Press, Boca Raton, Chap II - Modelling of Flat Rolling Processes, pp 127–139